Computer Simulation of Block Copolymer/Nanoparticle Composites

Andrew J. Schultz, Carol K. Hall,* and Jan Genzer

Department of Chemical and Biomolecular Engineering, North Carolina State University, Box 7905, Raleigh, North Carolina 27695-7905

Received February 14, 2004; Revised Manuscript Received November 26, 2004

ABSTRACT: Discontinuous molecular dynamics simulation is used to study the phase behavior of diblock copolymer/nanoparticle composites. The copolymers are modeled as chains of tangent hard-spheres with square shoulder repulsions between unlike species, while the nanoparticles are modeled as hard-spheres with a square shoulder repulsion with one of the copolymer blocks. The resulting phase diagrams are presented for composites containing nanoparticles of various sizes and interaction strengths and include lamellae, perforated lamellae, cylinders, and disordered phases. Composites containing large nanoparticles also exhibit two-phase coexistence between different copolymer phases or between a copolymer phase and a nanoparticle phase, depending on the nanoparticle interaction strength. We also present concentration profiles perpendicular to the lamellar interface for nanoparticles of different sizes and interaction strengths. Neutral nanoparticles concentrate at the interface between copolymer domains, while interacting nanoparticles concentrate within the favorable domain. The larger nanoparticles are more easily localized but have less impact on the copolymer concentration profiles. The lamellar spacing increases with nanoparticle volume fraction for interacting nanoparticles but decreases with nanoparticle size. The locations of the phase transitions are in qualitative agreement with theoretical predictions, but the concentration profiles are inconsistent with theoretical predictions. The variation of the spacing with nanoparticle volume fraction is consistent with experimental data.

1 Introduction

Particles have long been added to polymers to improve their physical properties, such as strength, toughness, and thermal behavior. Nanoparticles have begun to replace larger particles in composite materials because they can impart different properties such as optical transparency yet, at the same time, provide property enhancements at lower loadings. Block copolymers form a variety of ordered structures on nanometer length scales,[1] allowing them to serve as a ordered matrix for nanoparticles which add functionality to the composite. The result is an ordered array of nanoparticles with potential applications including magnetic storage media, photonic crystals, or high-surface-area catalysts.

Considerable effort has been devoted to theoretical and computer simulation studies of neat block copolymer phase behavior. Theories are capable of predicting the locations of the order−disorder transition (ODT),[2−4] the point where an ordered structure dissolves into a disordered one, and the order−order transitions (OOT),[2,3,5,6] the spacing between periodic repeat units such as lamellae, the interfacial thickness, and the energy and entropy[5−10] all as functions of the copolymer chain length (N), the volume fraction of each component (f), the interaction strength (χ), and the volume fraction of copolymers in the solution (ϕ_C). Computer simulation has also been used to study block copolymer phase behavior. Previous computational research has focused on the location of the ODT,[10,11] the structural spacing of lamellae,[10,12] and the transitions between the many ordered structures, including lamellae, perforated lamellae, cylinders, and BCC spheres.[13] We mapped out block copolymer phase diagrams as a function of χ, N, f, and η, the volume fraction occupied by copolymer beads,[14] using the so-called box length search algorithm,[15] which allowed us to efficiently determine the optimal box length for the block copolymer structures. The algorithm also allowed us to more accurately determine structural properties of ordered structures, including the periodic spacing, internal energy, and entropy of lamellar structures.

Experimental research on block copolymer/nanoparticle composites has mainly focused on the behavior of the nanoparticles within the block copolymer matrix. Hamdoun et al. studied a system containing nearly symmetric polystyrene−polybutylmetacrylate PS-*b*-PBMA block copolymer (M_w = 82K) and maghemite (γ-Fe_2O_3) nanoparticles of diameter 3.5 nm covered with short PS chains. They used atomic force microscopy to determine the variation of the lamellar spacing with nanoparticle volume fraction and used that, in conjunction with a simple theory, to infer that the nanoparticles were distributed throughout the PS domain rather than concentrated in the middle of the domain.[16] Later, Lauter-Pasyuk et al. used neutron reflectivity to study the same system but with longer chains (M_w = 135K and 170K) and larger nanoparticles (4 and 6 nm). Contrary to the Hamdoun et al. results for shorter chains and smaller nanoparticles, their data suggested that small nanoparticles tend to concentrate near the PS−PBMA interface, while large nanoparticles tend to concentrate in the center of the PS domain.[17] Bockstaller et al. investigated nanocomposites consisting of PS-*b*-PEP copolymer with gold nanoparticles and silica nanoparticles, both coated with aliphatics that preferred the PEP domain. The lamellar domain size of the copolymer was found to be 80−100 nm, the gold nanoparticles were 3.5 nm, and the silica nanoparticles were 21.5 nm. TEM images of the nanocomposites showed that the small gold nanoparticles localize near the lamellar interface, while the large silica nanoparticles prefer the center of the PEP domain.[18] Jain et al. studied systems containing polystyrene-*b*-polyisoprene and spherical, rodlike,

* Author to whom correspondence should be addressed. E-mail: hall@eos.ncsu.edu.

10.1021/ma0496910 CCC: $30.25
Published on Web 02/19/2005

or platelike nanoparticles. They used SAXS to determine the ODT temperature and found that the nanoparticles broadened the transition and shifted it to lower temperatures. The rodlike nanoparticles lowered the transition temperature the most.[19]

Computer simulation and theory have also been applied to block copolymer nanoparticle composites. Wang, Nealey, and de Pablo performed lattice Monte Carlo simulations to examine the position of a single spherical or cubic nanoparticle within a lamellae-forming symmetric block copolymer of length 24. They found that both large and small neutral nanoparticles were preferentially located at the copolymer interface, while a small nanoparticle that preferred component A of the copolymer was preferentially located within domain A. They also found that a large nanoparticle that preferred component A had little preference to stay in any one place, but they attributed this to the simulation method and the system size, which was larger than in their simulations with small nanoparticles.[20] Huh, Ginzburg, and Balazs performed lattice Monte Carlo simulations to examine the phase behavior of a composite containing block copolymers of length 32 and volume fractions $f = 0$ to 0.5, and cubic particles of widths 1 or 3 lattice sites that preferred one of the blocks. At $\chi N \approx 50$, they found that the nanoparticles were distributed throughout the preferred domain at low concentrations; as the nanoparticle concentration increased, the preferred domain swelled, eventually inducing transitions to cylinders and then to disorder. The larger nanoparticles precipitated into a particle-rich phase at high concentration. They also developed a strong segregation theory to predict the phase behavior of block copolymer/nanoparticle composites over a wide range of parameters and found reasonable agreement with their simulation results. This theory also predicts the stability, over a narrow range of parameters, of nanoparticle domains formed within one of the copolymer domains.[21] Later, Thompson, Ginzburg, Matsen, and Balazs studied block copolymer/nanoparticle composites using a theory that combined a self-consistent field theory (SCFT) for the block copolymers and a density functional theory for the nanoparticles. They found that the larger nanoparticles concentrated in the center of the preferred domain, while the smaller nanoparticles concentrated nearer the interface, which is consistent with some of the experimental observations.[17,18] In lamellae, the nanoparticles formed ordered nanosheets (monolayers or bilayers), while in cylinders, they formed helical or ring structures. Although nanoparticles also concentrated within the BCC spherical domains, they did not order within the spheres.[22,23] Chervanyov and Balazs used mean field theory to investigate the effect of particle size and shape on the ODT. They found that the ODT temperature decreases with nanoparticle concentration and also with the surface area-to-volume ratio.[24] Lee, Shou, and Balazs studied block copolymer/nanoparticle composites confined between walls using SCFT theory and found that the perpendicular or parallel orientations of lamellae were preferred, depending on the nanoparticle concentration, size, and strength of the interaction with the copolymers or walls.[25]

In this paper, we describe the results of discontinuous molecular dynamics (DMD) simulations of symmetric block copolymer/nanoparticle composites. The block copolymer is modeled as a chain of 20 hard-spheres of diameter σ_C with an square shoulder repulsion of strength ϵ_{AB} between A and B copolymer segments. The use of a repulsive potential between unlike species is equivalent to attractive interactions between like species but is computationally more efficient. The nanoparticle is modeled as a single sphere with a range of diameters, $\sigma_P = \sigma_C$, $2\sigma_C$, and $4\sigma_C$. The nanoparticles can have neutral interactions with the copolymer components or can repel one of the components with strength, $\epsilon_{AP} = \epsilon_{AB}$ or $2\epsilon_{AB}$. Repulsive potentials are used again for computational efficiency. The packing fraction, η, is fixed at 0.35, and the box length search algorithm described in ref 15 is used to accommodate the periodic structures.

Phase diagrams in the nanoparticle volume fraction vs χ_{AB} plane have been constructed on the basis of our simulation results at different values of σ_P and ϵ_{AP}. We find disordered, lamellar, perforated lamellar, and cylindrical structures. We also find a two-phase region at low temperature and high nanoparticle volume fraction. These phase diagrams are qualitatively consistent with the Monte Carlo simulations and strong segregation theory results of Huh et al.

We have also calculated the average concentration profiles in copolymer/nanoparticle systems with different values of σ_P and ϵ_{AP}. Neutral nanoparticles tend to concentrate at the AB interface to screen AB interactions, while nanoparticles that repel component A concentrate in the center of domain B, pushing component B out from the middle of its domain. The nanoparticles' tendency to concentrate in one area increases with nanoparticle size, while their impact on the concentration profiles of the copolymer blocks decreases with increasing nanoparticle size. These results are qualitatively different from self-consistent field theory predictions, which state that the nanoparticles are much more strongly localized, with larger nanoparticles forming monolayer sheets in the center of the preferred domain and smaller nanoparticles forming bilayer sheets with one sheet next to each interface.

Finally, we have calculated the periodic spacing as a function of σ_P and ϵ_{AP}. The neutral nanoparticles decrease the periodic spacing, while nanoparticles with a preference for domain B increase the periodic spacing. This increase in periodic spacing is caused by the swelling of domain B by the nanoparticles but is partially offset by contractions of domain A. The effect of the nanoparticles on the periodic spacing and the sizes of domains A and B decreases with increasing nanoparticle size.

The remainder of this paper is organized into the following sections: Section 2 describes the models used for the block copolymers and nanoparticles and the simulation techniques that we have used. Section 3 presents the phase diagrams constructed from our simulation data. Section 4 presents the concentration profiles for copolymer components A and B and for the nanoparticles. Section 5 presents the variation of the periodic spacing and the size of the copolymer domains as a function of σ_P and ϵ_{AP}. In Section 6, we summarize our results.

2. Copolymer and Nanoparticle Models and Simulation Technique

2.1. Copolymer and Nanoparticle Model. The block copolymer model used in our simulations is the same as the one described in our previous work on neat block copolymers in ref 14. The copolymer is modeled as a flexible chain of

spheres (beads) of components A and B, all with a hard-sphere diameter, σ_C. Additionally, beads of component A and B repel each other with a square-shoulder potential of strength ϵ_{AB} that extends to distance $2\sigma_C$. The nanoparticles are modeled as single spheres, with a hard-sphere diameter, σ_P, and a hard core interaction with copolymer beads at separations of $(\sigma_C + \sigma_P)/2$. The nanoparticles also have a square shoulder repulsion with component A beads of strength ϵ_{AP} that extends to a distance of $\sigma_C + (\sigma_P + \sigma_C)/2$. In the remainder of this paper, we will refer to reduced parameters for the nanoparticle size and interaction strength as $\sigma_P^* \equiv \sigma_P/\sigma_C$ and $\epsilon_P^* \equiv \epsilon_{AP}/\epsilon_{AB}$. For the simulations described in this paper, we have set σ_P^* to 1, 2, and 4, and ϵ_P^* to 0, 1, and 2. Justification for our parameter choices is the following. Although a system whose nanoparticles are equal in size to the copolymer beads might seem to be more representative of a copolymer solution than a nanocomposite, we have used this nanoparticle size as a reference to help us interpret the behavior of larger nanoparticles. While nanoparticles in experiments can have more complex and more repulsive interactions with the polymer species than we present here, the nanoparticles are often coated with one of the copolymer species, making it somewhat soluble in that copolymer block. Our choice of $\epsilon_{BP} = \epsilon_{BB} = 0$ for the interaction strength between the nanoparticles and the B component of copolymer is a simplified representation of this situation. The hard-sphere and square shoulder interactions of the nanoparticle can also be thought of as a simplified core/shell model for the polymer-coated nanoparticles.

2.2. DMD Simulation Algorithm. In a DMD simulation, particles experience collisions when they hit a discontinuity in the potential. Between collisions, particles experience linear trajectories, making the simulation technique faster than traditional molecular dynamics simulations, which generally require a small integration time step. The postcollision velocities can be found by solving the collision dynamics equations. To treat chains of beads effectively, Rapaport created bonds between beads by restricting the distance between adjacent beads to lie between σ and $\sigma(1 + \delta)$.[26] Bellemans later extended this model so that the distance between adjacent beads can lie between $\sigma(1 - \delta/2)$ and $\sigma(1 + \delta/2)$, making the average bond length σ.[27]

The DMD code we use is based on code originally developed by Smith et al.,[28] which we have extended to efficiently simulate mixtures of monomers, polymers, and copolymers. It also includes a search algorithm which finds the box lengths for a periodic structure that minimize its free energy by tracking the difference in the pressure between different dimensions. For instance, if the pressure in the x direction is greater than the pressure in the y or z direction, the x box length is increased and the y and z box lengths are decreased, so that the total volume of the system is held constant. Such box length changes are performed until the pressure in each direction is equal. This algorithm is used in the research reported here to determine the periodic spacing of copolymer lamellae and hexagonal arranged cylinders. Without such an algorithm, the box length can sometimes be inappropriate, making thermophysical properties that are sensitive to the box length, such as internal energy or radius of gyration, inaccurate. In simulations near a phase transition, the use of the wrong box length could lead to misidentification of the stable phase.

2.3. Relating Model Parameters to Commonly Accepted Molecular Parameters. To quantitatively relate our model to other models from simulation, theory, and experiment, we must define appropriate reduced parameters. First, the interaction strength between A and B particles, χ_{AB}, is defined as

$$\chi_{AB} \equiv z\epsilon_{AB}/k_BT \tag{1}$$

where z is the average number of nonbonded neighbors within the interaction distance, k_B is Boltzmann's constant, and T is the temperature. On the basis of our simulation data for neat block copolymer chains, $z = 19.36$. From our previous study of neat block copolymers, we know that the copolymer's ODT occurs between $\chi_{AB}N = 24.2$ and 25.8, so we have considered $\chi_{AB}N$ values from 27.7 to 48.4 in order to focus on ordered structures.

The second important parameter in our model is the size of the particles. As a measure of the nanoparticle size relative to the size of a copolymer chain, we calculate the ratio between the nanoparticle diameter and the athermal end-to-end distance of the copolymer chain, $R_0 \equiv \sqrt{\langle R^2 \rangle}$. For our copolymer model, $R_0/\sigma_C = 5.69$, so that $\sigma_P^* = 1$, 2, and 4 correspond to $\sigma_P/R_0 = 0.176$, 0.352, and 0.703, respectively.

Mean field theories contain a parameter χ_{AP} that describes the interaction between nanoparticles and the unfavorable copolymer component,[21,22] but we are unable to directly relate this parameter to any parameters in our copolymer/nanoparticle composite model. The χ_{AP} used in mean field theories is a measure of the local interaction strength in the overlap region between nanoparticles and copolymer. It is unclear what such a value would mean in the context of our model since our simulation technique strictly enforces excluded volume constraints between the nanoparticle and copolymer. Instead of calculating a value of χ_{AP} to quantify the nanoparticle interaction strength, we have varied $\epsilon_P^* \equiv \epsilon_{AP}/\epsilon_{AB}$ from 0 to 2 in order to investigate the effect of the interaction strength. Varying the interaction strength over this broad range means that we are exploring a range of parameter space that is likely to overlap the parameter space explored by others, although we cannot pinpoint where our interaction parameters match theirs. The average number of interacting neighbors is the other factor that affects χ. In our model, the range of the nanoparticle square shoulder is such that, at athermal conditions and infinite dilution, there are 21, 38, and 88 copolymer beads within the interaction distance of nanoparticles with diameter $\sigma_P^* = 1$, 2, and 4, respectively.

2.4. Simulation Methods. Because of the broad range of parameters that can play an important role in the phase behavior and properties of copolymer/nanoparticle composites, we have chosen to narrow our investigation to the case of symmetric block copolymer ($f = 0.5$) chains containing 20 beads at a packing fraction, $\eta = 0.35$, where η is the fraction of volume in the system occupied by nanoparticles, $\eta \equiv \pi\sum_i N_i\sigma_i^3/6$, V is the volume, N_i is the number of beads of species i in the system, and σ_i is the diameter of a species i bead. The volume fraction of nanoparticles, $\phi_P \equiv N_P\sigma_P^{*3}/(N_C + N_P\sigma_P^{*3})$, was varied from 0.0 to 0.4 by replacing copolymer chains with nanoparticles which occupied the same volume. At each condition, a simulation was first performed on a small system whose volume would hold 4000 copolymer beads ($V/\sigma_C^3 = 5984$) for systems with $\sigma_P^* = 1$ and 2 and 6400 copolymer beads ($V/\sigma_C^3 = 9574$) for systems with $\sigma_P^* = 4$. The box length search algorithm described previously was used to determine the optimal box length for any ordered structure that formed. Once the optimal box length was determined, the box length search algorithm was stopped and a new simulation was started at constant volume for $t^* \equiv t\sqrt{k_BT/m}/\sigma_C = 20\,000$ reduced time units, while properties such as the potential energy, radius of gyration, end-to-end distance, and structure factor were sampled. Although the system size used here is relatively small and accommodates only one repeat unit of the periodic structures that formed, we found no statistical difference in the properties of structures in the small system and one eight times as large, so long as the structure was not near a phase transition. If the system was near a phase transition, we verified that the small system size was not preventing a phase transition by replicating two copies of the unit subcell in every direction and continuing the simulation with a system eight times larger than the original (small) system. Total CPU time on a single CPU of an AMD Athlon MP 2000+ needed to simulate at a single condition ranged from 15 h for a small system to 10 days for a large system near a phase transition.

When mapping out phase diagrams, the stable phase at each temperature and nanoparticle volume fraction was determined by visual inspection of the final structure. Rather than use a

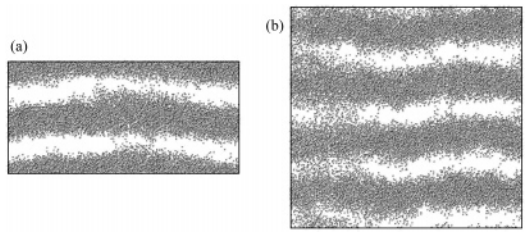

Figure 1. Snapshots of the simulation structure for $\sigma_P^* = 4$, $\epsilon_P^* = 1$, $\chi_{AB}N = 48.4$, at (a) $\phi_P = 0.2$ showing a lamellar structure and (b) $\phi_P = 0.3$ showing a two-phase system with both lamellae and disorder.

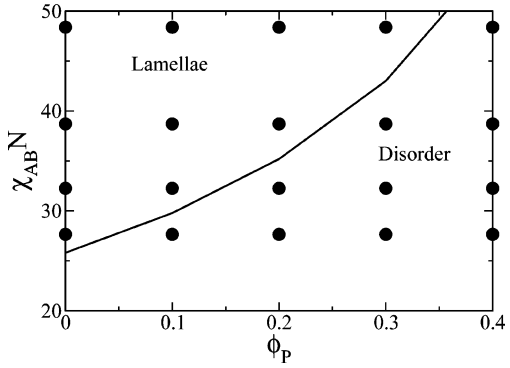

Figure 2. Block copolymer/nanoparticle phase diagrams from simulation for neutral nanoparticles plotted in $\chi_{AB}N$ vs ϕ_P space.

random initial configuration as the starting point for each condition, we started with the final structure from another condition and either lowered the temperature or increased the volume fraction of nanoparticles. This substantially increased the range of parameters that we could investigate, at the cost of seeing transitions in only one direction. We therefore tested the reversibility of representative phase transitions by conducting sweeps in the opposite direction. In every case we tested, except one (to be described), we found the phase transition to be reversible.

To illustrate the usefulness of visual inspection in determining the structural identity in our simulations, we show simulation snapshots of two systems at similar conditions but exhibiting different phase behavior in Figure 1. The snapshots contain only component A, using a diameter of 0.4 for clarity. Both systems contain nanoparticles of size $\sigma_P^* = 4$, nanoparticle interaction strength $\epsilon_P^* = 1$, and were performed at $\chi_{AB}N = 48.4$. The system in Figure 1a has a nanoparticle volume fraction of $\phi_P = 0.2$, and the system in Figure 1b has a nanoparticle volume fraction of $\phi_P = 0.3$. The snapshot in Figure 1a shows clear layering throughout the system. By examining each layer separately, we determined that the structure was perforated lamellae. The snapshot in Figure 1b shows clear layering in the right side of the simulation box but a more disordered structure in the left side. Using nanoparticle density profiles reconstructed from the structure factor, we also determined that the area containing relatively disordered block copolymers also contained a higher concentration of nanoparticles. This indicated phase separation between a nanoparticle-poor perforated lamellar and a nanoparticle-rich disordered copolymer phase.

3. Phase Diagrams

We have constructed phase diagrams in $\chi_{AB}N$ vs ϕ_P space, where ϕ_P is the volume fraction of nanoparticles. The phase diagram for neutral nanoparticles is shown in Figure 2, with each point in the phase diagram corresponding to a simulation and a line drawn to identify the resulting phase boundary. The phase diagram contains lamellae at high values of $\chi_{AB}N$ and low values of ϕ_P and disorder at low values of $\chi_{AB}N$ and high values of ϕ_P. The phase diagram for neutral nanoparticles is the same for all nanoparticle sizes considered. In fact, we found the same phase diagram for neat block copolymers if we simply lowered the packing fraction from $\eta = 0.35$, the value at which Figure 2 was constructed to $\eta = 0.35(1 - \phi_P)$ at every value of ϕ_P. In other words, instead of removing the chains and replacing them with nanoparticles to keep the packing fraction constant at $\eta = 0.35$, we removed the chains without replacing them with nanoparticles. Effectively, the neutral nanoparticles fill in voids between the copolymers but do not alter the copolymer structure enough to cause a different phase to have the lowest free energy. This result is not consistent with the theoretical predictions of Chervanyov and Balazs, who found that $\chi_{AB}N$ increased with increasing nanoparticle size. However, they found that nanoparticles increased $\chi_{AB}N$ by less than 2% for $\phi_P = 0.10$ over the range they investigated, which our coarse-grained $\chi_{AB}N$ sampling would not detect.

We also constructed phase diagrams for nanoparticles that repel component A with strength $\epsilon_P^* = 1$ and 2 and nanoparticle diameters $\sigma_P^* = 1$, 2, and 4. These are shown in Figure 3. In contrast to the phase diagram for neutral nanoparticles, which features only one ordered structure—the lamellar phase—this phase diagram contains several ordered structures that are stabilized by the repulsive nanoparticles, which tend to swell domain B. At $\sigma_P^* = 1$, shown in Figure 3a and d (column 1), perforated lamellae and cylinders are stable between lamellae and the disorder phase. However, at $\sigma_P^* = 2$, shown in Figure 3b and e (column 2), only perforated lamellae are stable between lamellae and disorder. The cylindrical phase is absent in the phase diagrams for nanoparticles with larger diameters $\sigma_P^* = 2$ (and 4) because the larger nanoparticles are less effective at swelling domain B than the smaller nanoparticles, as we will show in Section 4.

Our simulation phase diagrams include the perforated lamellae phase instead of the gyroid phase observed in experimental[29,30] and theoretical studies[8] of neat diblock copolymers. This is consistent with the behavior that we found for copolymer systems in the absence of nanoparticles; those systems also formed perforated lamellae but not gyroid.[14] Although it is possible that adding nanoparticles could stabilize the gyroid phase, we would expect this to occur for nanoparticles that localize within the minority component, where they could relieve packing frustration at the gyroid nodes.[8] In the present work, the nanoparticles swell what is effectively the majority domain, so we would not expect the nanoparticles to stabilize the gyroid phase.

Although we have plotted lamellae as the stable phase at $\sigma_P^* = 1$, $\epsilon_P^* = 2$, $\phi_P = 0.3$, and $\chi_{AB}N = 48.4$ in Figure 3d, cylinders cooled from $\chi_{AB}N = 38.7$ did not transform to lamellae, making it difficult to identify the most stable phase at this condition. This metastability is consistent with our previous work on neat diblock copolymers described in ref 14, where cylinders did not transform to lamellae when cooled, even when lamellae had the lower free energy.

We now focus on the phase behavior of nanoparticles with $\epsilon_P^* = 2$, shown in Figure 3d–f (second row). The primary effect on the phase diagram of increasing the nanoparticle interaction strength, ϵ_P^*, from 1 to 2 is

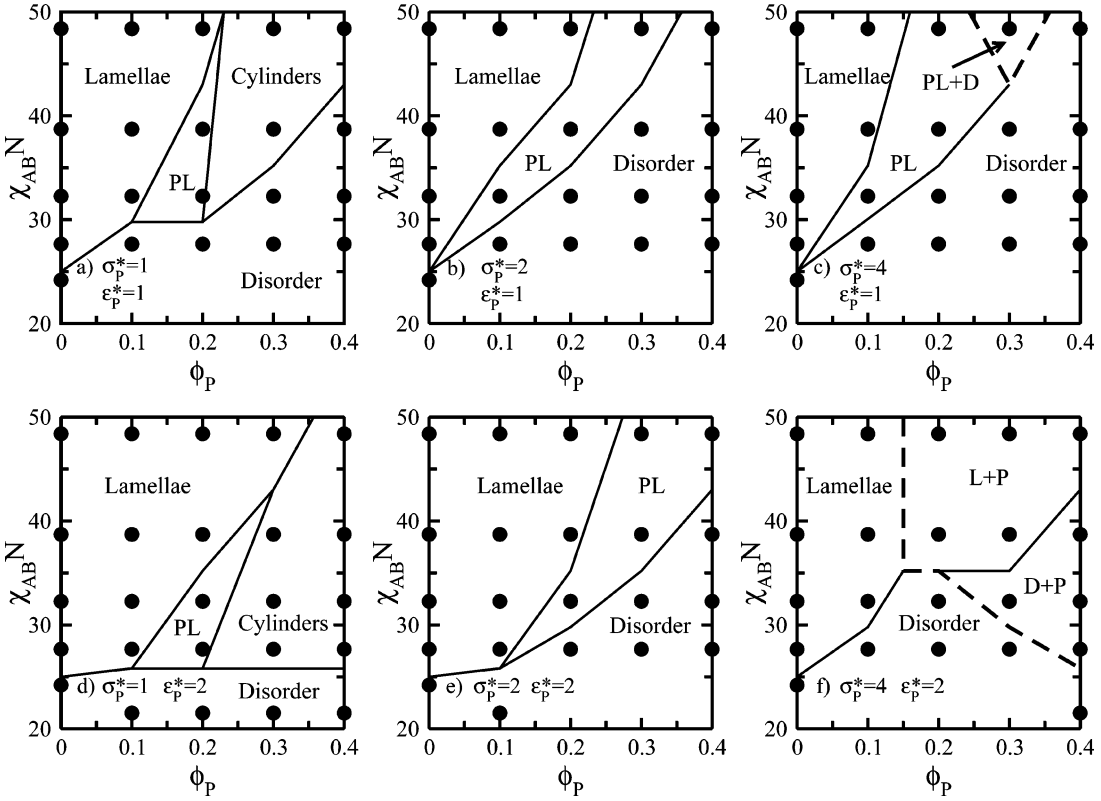

Figure 3. Block copolymer/nanoparticle phase diagrams from simulation, plotted in $\chi_{AB}N$ vs ϕ_P space for $\sigma_P^* = 1$, 2, and 4 (columns 1, 2, and 3) and $\epsilon_P^* = 1$ and 2 (rows 1 and 2).

that the phase transitions are shifted downward to lower values of $\chi_{AB}N$. For example, consider the location of the ODT. At $\sigma_P^* = 1$ and $\phi_P \leq 0.4$ and at $\sigma_P^* = 2$ and $\phi_P = 0.1$, the nanoparticles with $\epsilon_P^* = 2$ stabilize the ordered structures at $\chi_{AB}N = 27.7$, where the structures with $\epsilon_P^* = 1$ are disordered. (Additional simulations were performed at $\chi_{AB}N = 21.5$, a value not considered for other values of σ_P^* and ϵ_P^* to verify that the ODT had not moved to even lower values of $\chi_{AB}N$ as the nanoparticle volume fraction increased. In each case, the simulations at $\chi_{AB}N = 21.5$ produced disordered structures). The reason for the stability of the ordered structures at low values of $\chi_{AB}N$ is that the small and strongly interacting nanoparticles disperse throughout the B domain, effectively increasing the repulsiveness of that domain for component A. These results are similar to SCFT predictions for diblock copolymer/homopolymer blends,[31] where addition of homopolymer which preferred one of the blocks to a disordered copolymer system increased the effective interaction between the blocks and induced ordering within the blocks.

The phase diagram for nanoparticles with $\sigma_P^* = 4$ and $\epsilon_P^* = 1$, shown in Figure 3c, is similar to the one for $\sigma_P^* = 2$ and $\epsilon_P^* = 1$ (Figure 3b), except that perforated lamellae are stable at $\chi N = 48.4$ and $\phi_P = 0.2$ and macrophase separation between disordered copolymers and perforated lamellae occurs at $\chi N = 48.4$ and $\phi_P = 0.3$. The perforations at $\phi_P = 0.2$ and $\chi N = 48.4$ are sparse, transient, and are accompanied by a slight localization of nanoparticles above and below the perforations. At the higher nanoparticle volume fraction, $\phi_P = 0.3$, the perforations become more stable and the localization of nanoparticles leads to holes in the two lamellar layers on top of one another. In other words, the nanoparticle localization in one perforation induces another perforation in the adjacent lamellar layer. To test if the system was attempting to macrophase separate, we doubled the system size to obtain four lamellar layers. In this larger system, the lamellar perforations grew in size and eventually became a disordered phase rich in nanoparticles that filled about half the box. The other half of the box still contained perforated lamellae, but with fewer nanoparticles. More accurate determination of the two-phase region and the properties of the two phases would require a much larger simulation box or a more appropriate simulation method for probing phase separation, such as Gibbs ensemble Monte Carlo.

Increasing the interaction strength at $\sigma_P^* = 4$ from $\epsilon_P^* = 1$ to $\epsilon_P^* = 2$ destabilizes the perforated lamellae and increases the size of the two-phase region, as shown in Figure 3f. However, in this case, since the nanoparticles are strongly interacting, one of the phases is a crystalline nanoparticle phase, indicated by the symbol P. Each point in the phase diagram's two-phase region corresponds to a system whose final structure contained a single cluster of nanoparticles. Although it is possible that these clusters would be dispersed if our system was much larger, we consistently saw growth of the clusters with increasing system size. Additionally, we would not expect such dispersed clusters to be stable because they would break up any copolymer ordering and raise the free energy of the system. The nanoparticles organize themselves on an fcc lattice within the clusters due to differences in the compressibility factor in the copolymer and nanoparticle phases. Although the system packing fraction at 0.35 is well below 0.5, the packing fraction where hard-spheres would normally crystallize, the nanoparticles crystallize in the clusters because the

compressibility factor is high. The compressibility factor in the nanoparticle phase is much higher than in the copolymer phase because the pressure in the two phases must be equal, but the molecular density of pure nanoparticles is less than one-third the density that a pure copolymer phase would have at the same packing fraction (because a nanoparticle is 64 larger than a copolymer bead and the chain is only 20 times larger). Since the nanoparticle−nanoparticle interactions are purely hard-sphere interactions, the crystallization transition is related directly to the compressibility factor and the higher compressibility factor in the nanoparticle phase induces crystallization.

We can compare our phase diagram for $\sigma_P^* = 1$ and $\epsilon_P^* = 1$ with the results of Huh et al., who conducted simulations at $\epsilon_{AB} = 1$ and $\chi N_{AB} \approx 50$, which is only slightly higher than the highest value we simulated, $\chi N_{AB} = 48.4$. For the case of $f_A = 0.5$ and small nanoparticles, they also found a transition from lamellae to cylinders. For larger cubic nanoparticles with a size of 3 lattice units, they found macrophase separation into a copolymer lamellar phase and a nanoparticle phase at $\phi_P = 0.2$. In our own simulations, nanoparticles with $\sigma_P^* = 4$, $\epsilon_P^* = 1$, and $\phi_P = 0.3$ induced macrophase separation into different copolymer phases instead of a copolymer phase and a nanoparticle phase, as seen by Huh et al. This difference in phase behavior between the Huh et al. results and our results is probably because the number of nanoparticle neighbors (and therefore the effective interaction strength) increases with nanoparticle size more slowly in our own system than in theirs. On a simple cubic lattice, the number of neighbors around their cubic nanoparticles scales with the square of the nanoparticle size. In our continuum model, the number of neighbors around our spherical nanoparticle increases approximately linearly with nanoparticle size. This difference means that their large nanoparticles of size 3 lattice units actually correspond to nanoparticles with a much stronger interaction strength in our model, where we do find macrophase separation into nanoparticle clusters as seen by Huh et al.

We can also make comparisons with the strong segregation theory of Huh et al. They calculated phase diagrams for $N = 50$, $\chi_{AB}N = 50$, and nanoparticles with diameter 2, 4, and 8 times the copolymer segment size. They predicted two-phase coexistence between lamellae at $\phi_P = 0.15$ and disorder at $\phi_P = 0.25$ for nanoparticles with a diameter of 2 and coexistence between lamellae at $\phi_P = 0.24$ and disorder at $\phi_P = 0.43$ for nanoparticles of diameter 4. In our simulations at $\chi_{AB}N = 48.4$, nanoparticles of diameter $\sigma_P^* = 2$ did not induce phase separation when $\epsilon_P^* = 1$ or 2. The nanoparticles with $\sigma_P^* = 4$ did induce phase separation into perforated lamellar and disordered phases when $\epsilon_P^* = 1$ and $\phi_P = 0.3$ and into lamellar and nanoparticle phases when $\epsilon_P^* = 2$ and $\phi_P \geq 0.2$. The predicted values of Huh et al. for ϕ_P at the lamellae to disorder transition are close to our simulation values, but the effect of nanoparticle size on the location of the lamellae to disorder transition is opposite to that seen in our simulations. In our simulations, the stability of the disordered structures increases as the nanoparticle size increases, but in the strong segregation theory, the stability of the disordered structures decreases as nanoparticle size increases. One contributing factor to this difference is that the structures of the disordered phase in our simulations and in the mean field model are different. Our simulated disordered structures have short range order with domains rich in component A or in component B but lack long range order, while the strong segregation theory of Huh et al. assumes that the disordered phase is completely homogeneous ($\phi_A(\mathbf{r}) = f_A(1 - \phi_P)$ and $\phi_B(\mathbf{r}) = (1 - f_A)(1 - \phi_P)$). Small nanoparticles have more difficulty being confined to the small A or B domains found in our disordered phase than the larger nanoparticles, which are more easily localized in a small area, as we will describe in Section 4. The increased localization of the large particles within domain B of the disordered phase makes the internal energy of the disordered phase with large nanoparticles lower than the internal energy of the disordered phase with small nanoparticles. However, the strong segregation theory of Huh et al. assumes that the disordered phase is homogeneous, which means that it does not account for the larger nanoparticles' ability to reside in small disordered domains.

4. Concentration Profiles

In this section, we report on the concentration profiles of copolymer components and nanoparticles in the composite structures described in the previous section. The concentration profiles were determined by performing a simulation (after the equilibrium structure was reached) to calculate the structure factor from snapshots taken periodically during the simulation. We then calculated a density profile from each structure factor and averaged the density profiles together, using the technique described in ref 32. This technique accounts for translation of the structure within the simulation box. Additionally, we determine the local volume fraction of component i, $\phi_i(x)$ by calculating the average (in one dimension) of the density, $\rho_i(x)$, from $x - \sigma_i/2$ to $x + \sigma_i/2$ weighted by the cross-sectional area an imaginary particle centered at x would have at position $x + \Delta x$.

$$\phi_i(x) = \frac{6}{\rho\sigma_i^3} \int_{-\sigma_i/2}^{\sigma_i/2} (\sigma_i^2/4 - (\Delta x)^2)\, \rho_i(x + \Delta x)\, \mathrm{d}(\Delta x)$$

We plot concentration profiles of one lamellar unit cell at $\chi_{AB}N = 48.4$ and $\phi_P = 0.2$ for each value of $\epsilon_P^* = 0$, 1, and 2 and $\sigma_P^* = 1$, 2, and 4 in Figure 4. The concentration profiles for neutral nanoparticles in Figure 4a, d, and g (first column) show that the nanoparticles preferentially localize near the copolymer interface, where they screen out unfavorable A−B interactions. This preference for the interface increases as the nanoparticle size is increased from $\sigma_P^* = 1$ to 2 but does not change significantly when the nanoparticle size is increased again from $\sigma_P^* = 2$ to 4. Nanoparticles with small size, $\sigma_P^* = 1$, have a volume fraction of 0.17 in the center of the A and B domains and 0.24 at the interface, while the larger $\sigma_P^* = 2$ nanoparticles have a volume fraction of 0.13 at the center of the A and B domains and 0.28 at the interface. The nanoparticles' tendency to localize at the interface more as the nanoparticle size is increased is entropically driven. It is much easier to place one large ($\sigma_P^* = 4$) nanoparticle at the AB interface than to place 64 small ($\sigma_P^* = 1$) nanoparticles in the same place. Although the nanoparticle concentration profile changes with nanoparticle size, the concentration profiles of the copolymer components for the different nanoparticle sizes are nearly identical, indicating that

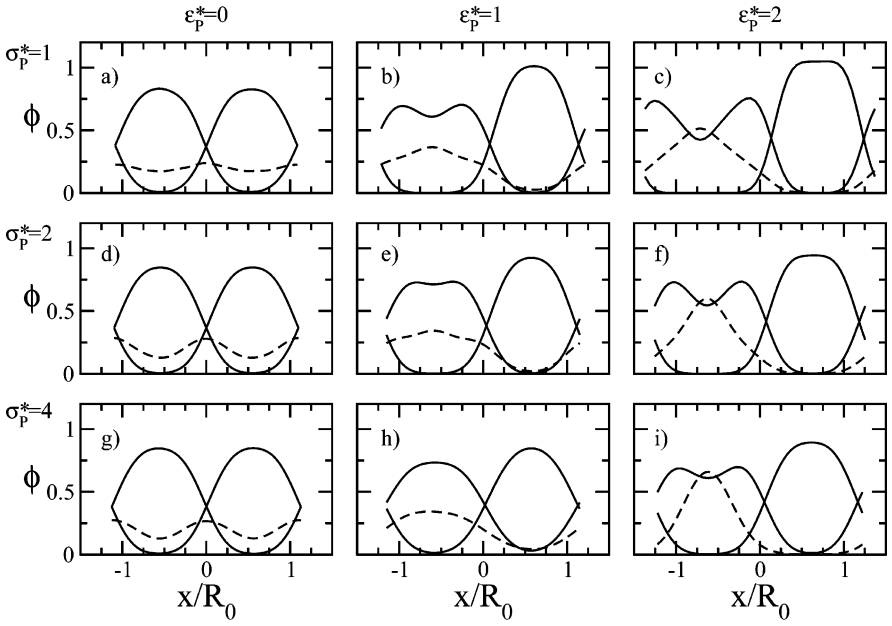

Figure 4. Concentration profiles for $\phi_P = 0.2$ and $\chi_{AB}N = 48.4$ for $\sigma_P^* = 1$, 2, and 4 (rows 1, 2, and 3) and $\epsilon_P^* = 0$, 1, and 2 (columns 1, 2, and 3). In each figure, domain B is on the left and domain A is on the right. Concentration profiles for copolymer components A and B are drawn with a solid line, and the nanoparticle concentration profile is drawn with dashed line.

the nanoparticles simply fill voids within the copolymer matrix without altering the copolymer structure.

The concentration profiles in Figure 4b, e, and h (second column) for $\epsilon_P^* = 1$ show that the nanoparticles with moderate repulsion alter the copolymer structure much more than the neutral nanoparticles do. The interacting nanoparticles distribute throughout the B domain with a slight preference for the domain center. Unlike the concentration profile for neutral nanoparticles, the nanoparticle concentration profile slightly broadens as the nanoparticle size is increased from $\sigma_P^* = 1$ to 2. Nanoparticles with small size, $\sigma_P^* = 1$, have a volume fraction of 0.36 in the center of domain B and 0.19 at the interface, while the larger $\sigma_P^* = 2$ nanoparticles have a volume fraction of 0.34 at the center of domain B and 0.22 at the interface. Although the nanoparticle concentration profile changes only slightly with increasing nanoparticle size, the copolymer concentration profiles are considerably more sensitive to nanoparticle size. With small σ_P^* nanoparticles, the concentration of component B has a significant dip in the center of domain B due to the nanoparticles' excluded volume. The concentration dip decreases in depth and then disappears when the nanoparticle size is increased to $\sigma_P^* = 2$ and finally to 4. This lack of a dip in the concentration profile of component B explains why the nanoparticle concentration profile is relatively insensitive to nanoparticle size. The increase in size of the nanoparticles by itself would lead to an increase in the nanoparticle localization in the center of domain B, but the lack of a dip in the concentration profile of component B removes part of the driving force for the nanoparticles to go there (the remaining driving force is the energetic repulsion from component A). The result is that the two effects mostly cancel one another, and the nanoparticle concentration profile does not change much as the nanoparticle size increases.

Finally, the concentration profiles for $\epsilon_P^* = 2$ in Figure 4c, f, and i (third column) show that the nanoparticles have a strong preference for domain B and localize in the domain center. Because the simulation of a large system at $\epsilon_P^* = 2$ and $\sigma_P^* = 4$ resulted in a phase separated structure, we have plotted concentration profiles from a smaller system which did not phase separate at the same values of ϵ_P^* and σ_P^*. Although not equilibrium structures, the profiles still help us to understand the effects of variation in σ_P^* and ϵ_P^*. The nanoparticles with diameter $\sigma_P^* = 2$ localize in domain B more than the nanoparticles with $\sigma_P^* = 1$, and the large nanoparticles with $\sigma_P^* = 4$ localize in the center even more. The greater localization in the center is due in part to the fact that the nanoparticle center must reside in the center of the domain to prevent the nanoparticle surface from penetrating the interface. The larger nanoparticles must go precisely to the center to achieve this not only because of their size but also because component A, which is less affected by the larger nanoparticles than the small nanoparticles, penetrates farther into domain B. As with the more weakly interacting nanoparticles, the dip in the concentration profile of component B becomes shallower as the nanoparticle size is increased. The resulting total volume fraction of particles at the center of domain B is greater than 1. The copolymers and large nanoparticles are able to pack more easily and fill more of the volume by mixing. We can then conclude that the anomalously high total volume fraction is an artifact of packing effects.

The concentration profiles from our simulations can be compared qualitatively with the concentration profile predictions made by Thompson et al. using self-consistent field theory and density functional theory, as well as with the experimental observations of Bockstaller et al.[18,22,23] Thompson et al. investigated systems with invariant polymerization index $\bar{N} = 1000$ and $\chi_{AB}N = \chi_{AP}N = 20$ and found that concentration profiles for large nanoparticles ($\sigma_P/R_0 = 0.6$) had a single peak in the center of the domain, while small nanoparticles ($\sigma_P/R_0 = 0.4$) formed two peaks near the copolymer interface. Bockstaller et al. found behavior consistent with

Thompson's theoretical predictions. They observed that small nanoparticles localize near the lamellar interface and large nanoparticles prefer the center of the PEP domain. The concentration profiles from our simulations of large nanoparticles do show localization at the center of domain B, but none of the concentration profiles from our simulation contained multiple nanoparticle peaks. Thompson et al. attributed the nanoparticle localization in the center of the domain or the edge to packing considerations.[23] Nanoparticles that were too large to have multiple layers within the domain formed only one peak, while smaller nanoparticles formed two peaks because both would fit within the domain. In our simulations, the nanoparticles are never sufficiently confined to make packing considerations important. The concentration profiles from our simulations are also much broader than the profiles from mean field predictions, which contain sharp peaks and crystalline ordering in two dimensions. It is likely that the difference in broadness between our results and theoretical predictions is due to the different parameters examined in their work and in our simulations. Although the nanoparticle diameter to copolymer end-to-end distance considered in the theory is similar to those we have found in simulation, the ratio of nanoparticle size to copolymer segment size in the study by Thompson et al. is much larger than that in our simulations since their chains are 50 times longer. The result is that the ratio of energetic to entropic driving forces in our simulations is much smaller than in the theoretical study. This energetic driving force in the theory effectively creates a steep free energy well that confines the nanoparticles to domain B, which sometimes forces them to form crystalline layers. Additionally, since the mean field theory finds the state with the lowest free energy (rather than an ensemble of states with low free energies), fluctuations in the nanoparticle positions are absent. Such fluctuations could break the tight layering and lead to broader particle concentration profiles.

5. Periodic Spacing

In this section, we report the lamellar spacing, d, of the structures described in Section 4. We also examine the size of the A and B domains in order to better understand the variation of the periodic spacing. We compare the periodic spacing with the experimental results of Hamdoun et al., who determined the periodic spacing of lamellae in thin films with and without nanoparticles. The periodic spacing from our simulations was calculated by dividing the simulation box length by the number of lamellar sheets. To calculate the sizes of the A and B domains, we located the AB interface in the concentration profiles from the previous section, as the point where $\phi_A = \phi_B$.

The scaled periodic spacing, d/R_0, from our simulation data for $\chi_{AB} = 48.4$ and $\phi_P = 0.2$ are plotted as a function of nanoparticle size σ_P^* at each value of ϵ_P^* in Figure 5. As a basis for comparison, the periodic spacing of a system with the nanoparticles removed (i.e., $\sigma_P^* = 0$) without replacing them with copolymers (a system of neat block copolymers with the packing fraction at 0.28) is $d = 2.25R_0$. The small nanoparticles with $\sigma_P^* = 1$ have the most impact on the periodic spacing. The small neutral nanoparticles decrease the periodic spacing to $2.17R_0$, the small nanoparticles with $\epsilon_P^* = 1$ swell the periodic spacing to $2.43R_0$, and the more strongly interacting small nanoparticles with $\epsilon_P^* = 2$ swell the

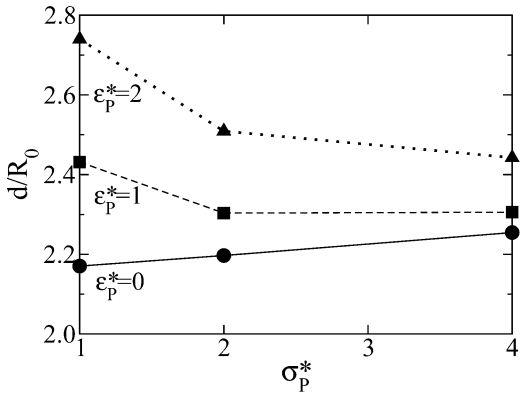

Figure 5. Lamellar spacing as a function of nanoparticle diameter for $\epsilon_P^* = 0$, 1, and 2, $\chi_{AB} = 48.4$ and $\phi_P = 0.2$.

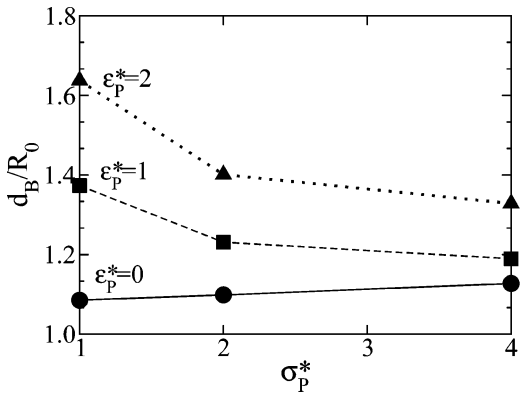

Figure 6. Size of domain B as a function of nanoparticle diameter for $\epsilon_P^* = 0$, 1, and 2, $\chi_{AB} = 48.4$ and $\phi_P = 0.2$.

periodic spacing to $2.74R_0$. The neutral nanoparticles decrease the periodic spacing by screening interactions between A and B copolymer at the copolymer interface, while interacting nanoparticles swell domain B, as we will discuss later. The strongly interacting nanoparticles with $\epsilon_P^* = 2$ increase the lamellar spacing more than nanoparticles with $\epsilon_P^* = 1$ because they localize more in the center of the B domain. As the nanoparticle size increases to $\sigma_P^* = 2$, the periodic spacing increases for the case of neutral nanoparticles and decreases for interacting nanoparticles. Increasing the nanoparticle size further to $\sigma_P^* = 4$, increases the periodic spacing for neutral nanoparticles and decreases the periodic spacing for $\epsilon_P^* = 2$ but has little effect when $\epsilon_P^* = 1$.

To better understand the dependence of the periodic spacing on ϵ_P^* and σ_P^*, we have calculated the size of the B and A domains and plot them in Figures 6 and 7, respectively. The variation of the size of domain B with ϵ_P^* and σ_P^* is almost the same as the variation in the periodic spacing (see Figure 5), indicating that the swelling of domain B is responsible for most of the variation in the periodic spacing. The size of domain A is more interesting because its size, which ranges from $d = 1.06R_0$ to $1.13R_0$ is generally less than it would be if the nanoparticles were removed, $d = 1.12R_0$. We can relate the contraction of domain A to the fact that the nanoparticles have a higher concentration at the interface than in domain A. Nanoparticles at the interface force apart copolymer chains, effectively stretching the lamellar sheets laterally (parallel to the lamellar interface) and creating voids within domain A. Domain A then contracts perpendicular to the interface to maintain constant density in the system if other nanopar-

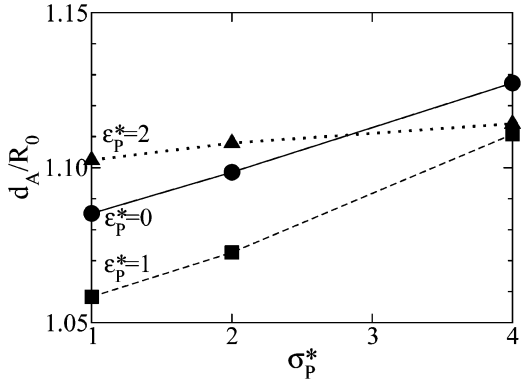

Figure 7. Size of domain A as a function of nanoparticle diameter for $\epsilon_P^* = 0$, 1, and 2, $\chi_{AB} = 48.4$ and $\phi_P = 0.2$.

ticles do not fill these voids. The neutral nanoparticles exist at the interface and within domain A but have a higher concentration at the interface (see Figure 4a, d, and g), so that domain A contracts. The concentration of nanoparticles with $\epsilon_P^* = 1$ is lower at the interface than it was for the case of neutral nanoparticles, but the interacting nanoparticles are nearly excluded from domain A (see Figure 4b, e, and h), so that domain A contracts much more than for the case of neutral nanoparticles. The concentration of nanoparticles with $\epsilon_P^* = 2$ is much lower at the interface (see Figure 4c, f, and i) than nanoparticles with $\epsilon_P^* = 1$, so that the contraction of domain A is small. As the nanoparticle size is increased, the size of domain A increases. The primary reason for this is the copolymers' general decrease in sensitivity to the nanoparticles as the nanoparticle diameter increases.

We can compare the variation of the lamellar spacing in our system with the experimental results of Hamdoun et al., who investigated the variation of the lamellar spacing with volume fraction of nanoparticles. They found that the spacing was approximately equal to $d = d_0(1 + p\phi_P)$, where p is a constant. In our system, we also found that the periodic spacing was approximately proportional to $1 + p\phi_P$ for the various values of ϵ_P^*, σ_P^*, and χ_{AB} that we examined (not shown). Hamdoun et al. found $p = 0.27$ for the case of 3.5 nm maghemite nanoparticles coated with polystyrene in PS-*b*-PBMA lamallae ($d_0 = 30$ nm). In our own simulations at $\phi_P = 0$, the lamellar spacing is $d = d_0 = 2.36R_0$. Using their value of p, our value of d_0, and their equation for the lamellar spacing as a function of ϕ_P, we can predict the lamellar spacing at $\phi_P = 0.2$ in our simulations. The predicted lamellar spacing of $2.48R_0$ is consistent with our simulation values of $d = 2.51R_0$ and $d = 2.44R_0$ for the periodic spacing of a nanoparticle/copolymer system at $\epsilon_P^* = 2$ and $\sigma_P^* = 2$ and 4, respectively.

6. Summary

We have performed discontinuous molecular dynamics simulations of block copolymer/nanoparticle composites at different values of χ_{AB} and nanoparticle volume fraction. On the basis of the simulation data, we constructed phase diagrams in χ_{AB} vs ϕ_P space at various values of ϵ_P^* and σ_P^* which exhibited lamellae, perforated lamellae, cylinders, and disordered structures. We also found phase coexistence between a crystalline nanoparticle phase and a copolymer phase for strongly interacting nanoparticles and between a nanoparticle-rich disordered phase and a nanoparticle-poor lamellar phase for more weakly interacting nanoparticles. The phase diagrams are qualitatively similar to previous simulation and theoretical results[21] and should provide further insight into how nanoparticles affect the phase behavior of block copolymers.

We also calculated concentration profiles for the copolymer components and nanoparticles in the lamellar phase. We found that the neutral nanoparticles tend to localize at the interface and nanoparticles that repel A tend to localize in domain B. This localization increased with nanoparticle size for neutral and strongly interacting nanoparticles but decreased with nanoparticle size for moderately interacting nanoparticles. We also found that the nanoparticles perturb the copolymer profiles less as the nanoparticle size increases. In contrast to theoretical predictions of sharp peaks in the nanoparticle concentration profile and a tendency of smaller nanoparticles to concentrate near the AB copolymer interface,[22] the simulation concentration profiles for interacting nanoparticles consistently had one broad peak in the center of domain B. We attribute these inconsistencies to the longer chain length used in the theoretical work and the inability to account for fluctuations in nanoparticle positions in the theory.

Finally, we have investigated the periodic spacing of lamellae containing nanoparticles. We found that small nanoparticles had the greatest effect on the periodic spacing, with the periodic spacing increasing as a function of nanoparticle interaction strength. As the nanoparticle size increased, the effect of the nanoparticles on the periodic spacing decreased. We also calculated the size of domains A and B and found that the variation in the size of domain B was similar to the variation in the periodic spacing but that domain A contracted with the addition of nanoparticles. We attribute this contraction to the higher concentration of nanoparticles at the AB interface than within domain A.

Although we have attempted to cover experimentally relevant ranges for the parameters in our model, we were limited in this regard by the short length of the copolymer chains in our simulations. The two length scales in our system, the size of a copolymer bead and the size of a chain, are not varied independently. Because of this, we cannot conclusively identify which of the two length scales is most important in determining the effect of the nanoparticle diameter on phase behavior or nanoparticle localization. Additionally, we are unable to quantitatively match the range of parameters accessed most often in previous experimental research, which have typically used nanoparticles of diameter 3−6 nm within copolymer domains of size 20−100 nm. This means that our largest nanoparticles are too large relative to the size of of our copolymer domain and our smallest nanoparticles are too small relative to our copolymer bead. By increasing the chain length, we can simulate nanocomposites with nanoparticles large enough relative to the copolymer bead without being too large relative to the copolymer domains.

Acknowledgment. This work was supported by the GAANN Computational Sciences Fellowship of the U. S. Department of Education and the Office of Energy Research, Basic Sciences, Chemical Science Division of the U. S. Department of Energy under Contract No. DE-FG05-91ER14181. Acknowledgment is made to the donors of the Petroleum Research Fund administered

by the American Chemical Society for partial support of this work.

References and Notes

(1) Bates, F. S.; Fredrickson, G. H. *Annu. Rev. Phys. Chem.* **1990**, *41*, 525.
(2) Leibler, L. *Macromolecules* **1980**, *13*, 1602.
(3) Fredrickson, G. H.; Helfand, E. *J. Chem. Phys.* **1987**, *87*, 697.
(4) Barrat, J.; Fredrickson, G. H. *J. Chem. Phys.* **1991**, *95*, 1281.
(5) Semenov, A. N. *Sov. Phys. JETP* **1985**, *61*, 733.
(6) Matsen, M. W.; Schick, M. *Phys. Rev. Lett.* **1994**, *72*, 2660.
(7) Whitmore, M. D.; Noolandi, J. *J. Chem. Phys.* **1990**, *93*, 2946.
(8) Matsen, M. W.; Bates, F. S. *J. Chem. Phys.* **1997**, *106*, 2436.
(9) Fredrickson, G. H.; Ganesan, V.; Drolet, F. *Macromolecules* **2002**, *35*, 16.
(10) Larson, R. G. *Macromolecules* **1994**, *27*, 4198.
(11) Besold, G.; Hassager, O.; Mouritsen, O. G. *Comput. Phys. Commun.* **1999**, *122*, 542.
(12) Murat, M.; Grest, G. S.; Kremer, K. *Macromolecules* **1999**, *32*, 595.
(13) Groot, R. D.; Madden, T. J. *J. Chem. Phys.* **1998**, *108*, 8713.
(14) Schultz, A. J.; Hall, C. K.; Genzer, J. *J. Chem. Phys.* **2002**, *117*, 10329.
(15) Schultz, A. J.; Hall, C. K.; Genzer, J. *J. Chem. Phys.* **2004**, *120*, 2049.
(16) Hamdoun, B.; Ausserr_e, D.; Cabuil, V.; Joly, S. *J. Phys. (France) II* **1996**, *6*, 503.
(17) Lauter-Pasyuk, V.; Lauter, H. J.; Ausserre, D.; Gallot, Y.; Cabuil, V.; Kornilov, E. I.; Hamdoun, B. *Physica B* **1998**, *241*, 1092.
(18) Bockstaller, M. R.; Lapetnikov, Y.; Margel, S.; Thomas, E. L. *J. Am. Chem. Soc.* **2003**, *125*, 5276.
(19) Jain, A.; Gutmann, J. S.; Garcia, C. B. W.; Zhang, Y.; Tate, M. W.; Gruner, S. M.; Wiesner, U. *Macromolecules* **2002**, *35*, 4862.
(20) Wang, Q.; Nealey, P. F.; de Pablo, J. J. *J. Chem. Phys.* **2003**, *24*, 11278.
(21) Huh, J.; Ginzburg, V. V.; Balazs, A. C. *Macromolecules* **2000**, *33*, 8085.
(22) Thompson, R. B.; Ginzburg, V. V.; Matsen, M. W.; Balazs, A. C. *Science* **2001**, *292*, 2469.
(23) Thompson, R. B.; Ginzburg, V. V.; Matsen, M. W.; Balazs, A. C. *Macromolecules* **2002**, *35*, 1060.
(24) Chervanyov, A. I.; Balazs, A. C. *J. Chem. Phys.* **2003**, *119*, 3529.
(25) Lee, J. Y.; Shou, Z.; Balazs, A. C. *Macromolecules* **2003**, *36*, 7730.
(26) Rapaport, D. C. *J. Chem. Phys.* **1979**, *71*, 3299.
(27) Bellemans, A.; Orban, J.; Belle, D. V. *Mol. Phys.* **1980**, *39*, 781.
(28) Smith, S. W.; Freeman, B. D.; Hall, C. K. *J. Comput. Phys.* **1997**, *134*, 16.
(29) Hajduk, D. A.; Takenouchi, H.; Hillmyer, M. A.; Bates, F. S. *Macromolecules* **1997**, *30*, 3788.
(30) Vigild, M. E.; Almdal, K.; Mortensen, K.; Hamley, I. W.; Fairclough, J. P. A.; Ryan, A. J. *Macromolecules* **1998**, *31*, 5702.
(31) Matsen, M. W. *Macromolecules* **1995**, *28*, 5765.
(32) Schultz, A. J.; Hall, C. K.; Genzer, J. in preparation.

MA0496910